Check for updates

ADVANCED SUSTAINABLE SYSTEMS
www.advsustainsys.com

Synthesis of Porous Clay Heterostructures Modified with SiO_2–ZrO_2 Nanoparticles for the Valorization of Furfural in One-Pot Process

*Salima Essih, Juan Antonio Cecilia, Carmen Pilar Jiménez-Gómez, Cristina García-Sancho, Francisco José García-Mateos, Juana María Rosas, Ramón Moreno-Tost, Francisco Franco, and Pedro Maireles-Torres**

The layered structure of two smectites (montmorillonite and saponite) are modified by the insertion of SiO_2–ZrO_2 nanoparticles, with a Si/Zr molar ratio of 5, to form porous clay heterostructures (PCHs). These PCHs exhibit a clear improvement of the textural and acid properties in comparison to the starting clays, due to the formation of a pillared structure and the presence of Zr species, which provide an increase in the amount of Lewis acid sites. These materials are studied in one-pot catalytic processes to transform furfural into valuable products, such as furfuryl alcohol, alkyl furfuryl ethers, alkyl levulinates or γ-valerolactone, depending on the experimental conditions. Thus, the use of milder reaction temperature (110 °C) favors the formation of furfuryl alcohol and alkyl furfuryl ethers, while higher temperatures (170 °C) promote the formation of alkyl levulinate and γ-valerolactone, as well as an increase in nondetected products associated to the formation of humins due to the polymerization of furfural and/or furfuryl alcohol.

1. Introduction

Lignocellulose, composed by lignin, cellulose, and hemicellulose, has emerged as a very abundant and sustainable source to replace the traditional fossil fuels.[1] These fractions can be separated and isolated by biological or thermochemical treatments to be valorized in subsequent steps.[2,3] Focusing on hemicellulose, this fraction is a heteropolymer formed by arabinoxylans, which can be depolymerized and dehydrated by a mild acid treatment to obtain furfural (FUR). These chemical is considered the second most produced compound (after ethanol) with an annual production volume of more than 280 ktons.[4,5]

It is possible to obtain a wide variety of high value-added chemicals from FUR, through hydrogenation, oxidation, decarbonylation, acetylation, condensation, among other reactions.[5–7] From an industrial viewpoint, about 62% of the FUR produced is used in the synthesis of furfuryl alcohol (FOL) by a hydrogenation reaction using copper chromite as catalyst.[7,8] Currently, the trend is the search and development of Cr-free catalysts, due to the serious concerns associated to the presence of Cr in copper chromite.[5,7] Thus, several transition metal-based catalysts (mainly, Cu, Ni, Pd, Pt) have been successfully used in FUR hydrogenation in vapor and liquid phases, although both conversion and selectivity patterns depend on the hydrogenating capacity and the acid/base character of the support.[5,7,9–11]

Catalytic transfer hydrogenation (CTH) has emerged as an alternative to metal-based catalysts in hydrogenation reactions. In the last decade, several metal oxides, such as Al_2O_3,[12–14] ZrO_2,[14–17] MgO,[18,19] or Fe_xO_y,[19,20] or zeolites modified with Zr^{4+},[21,22] Sn^{4+},[23,24] or Hf^{4+},[25] have shown a suitable catalytic performance for the synthesis of FOL through CTH. In all cases, Lewis acid sites promote the hydrogen catalytic transfer from alcohols (mainly, secondary alcohols) to a carbonyl group, through a six-membered intermediate.[26,27]

Besides the synthesis of FOL, one of the greatest challenges is obtaining other valuable chemicals, through several consecutive reactions (one-pot processes), with high yields. In the case of FUR valorization, the formation of alkyl furfuryl ether, alkyl levulinates or γ-valerolactone has been reported.[28,29] The selectivity pattern is modulated by the amount and strength of Lewis and Brönsted acid sites, as well as the reaction temperature and time. Generally,

S. Essih, J. A. Cecilia, C. P. Jiménez-Gómez, C. García-Sancho, R. Moreno-Tost, F. Franco, P. Maireles-Torres
Departamento de Química Inorgánica, Cristalografía y Mineralogía (Unidad Asociada al ICP-CSIC)
Facultad de Ciencias
Universidad de Málaga
Campus de Teatinos, Málaga 29071, Spain
E-mail: maireles@uma.es
F. J. García-Mateos, J. M. Rosas
Departamento de Ingeniería Química
Facultad de Ciencias
Universidad de Málaga
Campus de Teatinos, Málaga 29071, Spain

The ORCID identification number(s) for the author(s) of this article can be found under https://doi.org/10.1002/adsu.202100453.

© 2022 The Authors. Advanced Sustainable Systems published by Wiley-VCH GmbH. This is an open access article under the terms of the Creative Commons Attribution-NonCommercial License, which permits use, distribution and reproduction in any medium, provided the original work is properly cited and is not used for commercial purposes.

DOI: 10.1002/adsu.202100453

these reactions have been carried out using Zr-based catalyst, mainly Zr-modified beta zeolites.[29–32]

Nevertheless, clay minerals have not been reported for the FUR valorization in one-pot processes, so these layered phyllosilicates have been selected as starting materials to tune their textural and acid properties. In this sense, a methodology to generate porosity in clays consists of incorporating a bulky organic cation in the interlayer space and then a silicon alkoxide polymerizes around it to form a silica structure between adjacent sheets. Finally, the calcination of the organic cation leads to a porous structure. These materials are known as porous clay heterostructures (PCHs).[33,34] The acidity of these PCHs can be modified by the coaddition of other heteroatoms (Ti, Zr or Al) as alkoxides in the synthesis step.[34–36] In this context, the present manuscript deals with the synthesis of PCHs with SiO_2–ZrO_2 pillars. The synthesis of PCHs leads to materials with high surface area while the incorporation of Zr would provide Lewis acid sites.[26,35] Moreover, Zr-modified zeolites and Zr-modified porous silica have been successfully used in Meerwein–Ponndorf–Verley reactions, even in one-pot (cascade) processes, to obtain high value-added chemicals, such as alkyl levulinates and γ-valerolactone.[28–32]

This work will contribute to the achievement of the Sustainable Development Goals promoted by the United Nations,[37] to the extent that it seeks to reduce our dependence on fossil resources (with high environmental impact) through the use of residual renewable biomass, without competition with the food market, to produce chemicals and biofuels, minimizing their impact on climate change. In addition, the development of biorefineries for the treatment of lignocellulosic waste, generated mainly in rural areas, will increase employment in these areas. Finally, phyllosilicates are abundant and widely spread on earth, which have been proposed as catalysts instead of materials requiring chemicals for their synthesis.

2. Results and Discussion

2.1. Catalyst Characterization

The crystallinity and mineralogical content of raw clays have been evaluated by X-ray diffraction (XRD) (**Figure 1**). The XRD patterns of both samples show a broad band with a maximum located about 2θ (°) = 6.7–6.9, which corresponds to basal reflection (d_{001}) values of 12.8–13.1 Å, typical of phyllosilicates with a TOT structure (smectites) with different hydration degree.[34,38] From these basal reflections, it is not possible to discern between dioctahedral and trioctahedral smectites, so it is necessary to draw on to d_{060} reflection. Thus, the d_{060} reflection of montmorillonite appears at 62.01° (1.49 nm), confirming the presence of a dioctahedral smectite.[39] In the case of saponite, d_{060} reflection is observed at 60.70° (1.52 nm), which denotes the existence of a trioctahedral smectite.[39] In addition, both raw clays are accompanied by some crystalline impurities: montmorillonite displays typical reflections of quartz, feldspars and gypsum, and dolomite, quartz and feldspars are present in saponite.[38]

The incorporation and subsequent calcination of silica and zirconia species give rise the porous clay heterostructure, which provokes the d_{001} reflection and other basal reflections

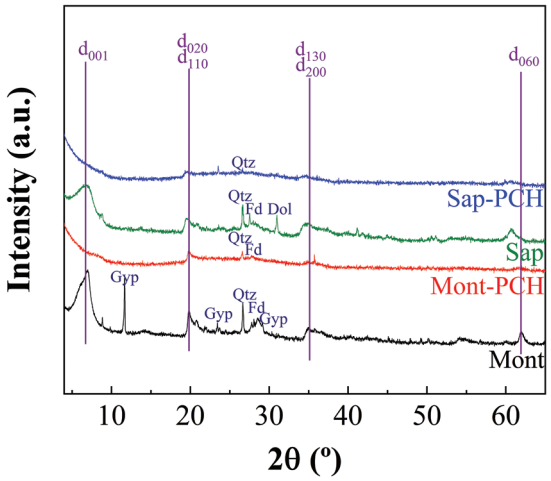

Figure 1. X-ray patterns of montmorillonite, saponite, and their respective porous clay heterostructures (PCHs). Acronyms: (Qtz: quartz, Gyp: gypsum, Fd: feldspar, Dol: dolomite).

disappear, while the intensity of nonbasal reflections decreases (Figure 1).[35] These data suggest the insertion of SiO_2–ZrO_2 pillars between adjacent sheets, although this could be accompanied by a random delamination of the TOT sheets, as was previously described in the literature.[35,40]

The chemical composition of the raw clays, determined by X-ray fluorescence (XRF) (**Table 1**), reveals the high concentration of Si. The main difference between Mont and Sap lies in the content of Mg and Al, because Mont is richer in Al (20.38 vs 7.70 wt% Al_2O_3) and Sap in Mg (23.63 vs 3.27 wt% MgO). In both raw clays, Na+ is the main cation located in the interlayer spacing, which compensates the charge deficiency of the TOT structure. The presence of Fe is ascribed to the partial substitution of silicon, whereas the presence of some impurities as Ca and K is also observed.

After the synthesis of PCH, a clear increase in the content of both Si and Zr is observed, because of the insertion of SiO_2–ZrO_2 nanoparticles between the layers. On the other hand, the decay of the Na content would confirm the cationic exchange of Na^+ by the hexadecyltrimethylammonium cation, which subsequent removal by calcination generates the porous structure.

The morphology of Mont and Sap and their respective PCHs was determined by transmission electron microscopy (TEM) (**Figure 2**). The images of Mont and Sap (Figure 2A,C) show that both raw clays are formed by the stacking of sheets, together with other structures without laminar morphology, which must be ascribed to the impurities detected by XRD (Figure 1). After the formation of PCHs (Figure 2B,D), the corresponding

Table 1. Chemical composition (wt%) of montmorillonite, saponite, and their respective porous clay heterostructures (PCHs) estimated by XRF.

Sample	SiO_2	Al_2O_3	Fe_2O_3	Na_2O	MgO	CaO	K_2O	TiO_2	ZrO_2	P_2O_5
Mont	65.34	20.38	4.70	3.36	3.27	2.05	0.48	0.30	0.03	0.03
PCH-Mont	78.72	8.65	2.06	0.28	1.38	0.17	0.18	0.13	8.38	0.02
Sap	57.71	7.70	2.83	2.86	23.63	2.49	1.87	0.41	0.02	0.01
Sap-PCH	75.58	2.89	1.11	0.18	8.95	0.80	0.66	0.16	9.62	0.01

© 2022 The Authors. Advanced Sustainable Systems published by Wiley-VCH GmbH

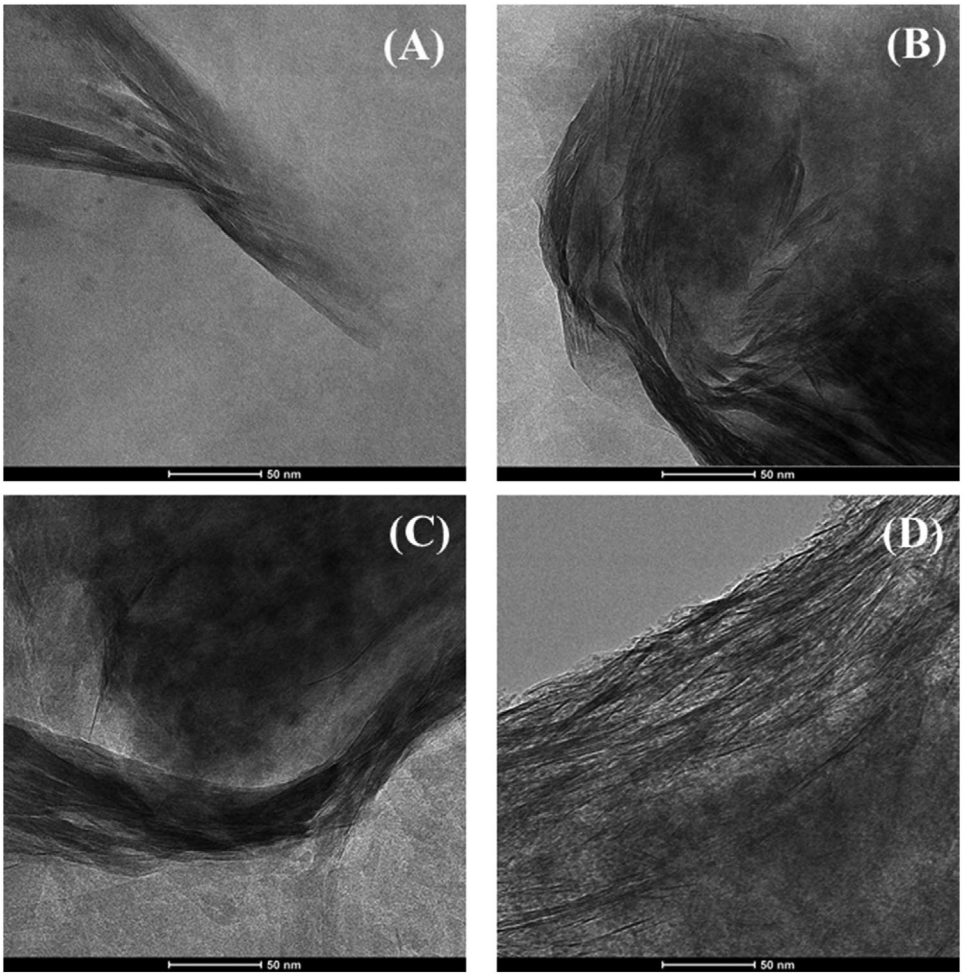

Figure 2. TEM images of A) Mont, B) Mont-PCH, C) Sap, and D) Sap-PCH.

images demonstrate that the layered structure is maintained, although the ordering worsens, probably due to a random displacement of the laminae by the formation of PCHs.[35]

On the other hand, the analysis by attenuated total reflectance (ATR) of hydroxyl stretching region evidences a vibration band at 3620 cm^{-1} in the case of montmorillonite, which is characteristic of Al-rich smectites with a high amount of silanol groups in octahedral sheets (**Figure 3**).[41] However, saponite exhibits a worse defined signal associated to silanol groups, attributed to [Mg_3OH] units located in octahedral sheets of trioctahedral smectites.[41] In the case of PCHs, it was not possible to observe any band in the −OH stretching region, which could be ascribed to the important dehydroxylation in both phyllosilicates due to the calcination of the organic template at 550 °C.[42]

The Si–O stretching vibrations appear between 960 and 985 cm^{-1}, whereas the M−OH bending vibration modes of dioctahedral and trioctahedral smectites are located in the 950–800 and 700–600 cm^{-1} regions, respectively.[42] The formation of the PCHs causes a shift of the Si–O stretching vibration modes at higher wavenumber due to the formation of amorphous SiO_2 between adjacent layers.[35] On the other hand, it is not possible to observe any band attributed to Zr species in the ATR spectra of PCHs.

Finally, both montmorillonite and saponite display a band located about 1640 cm^{-1}, which is attributed to bending modes of water molecules. However, this band is hardly observed for

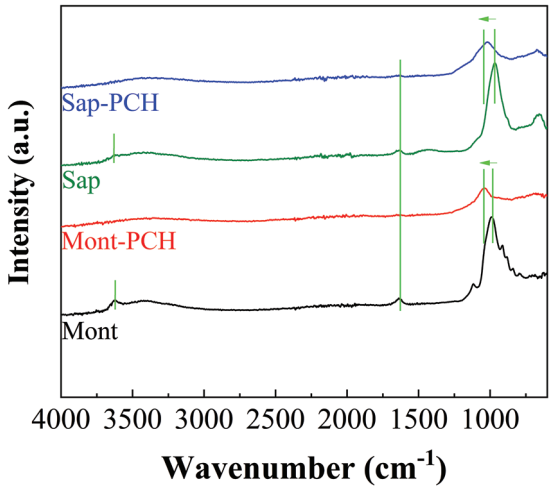

Figure 3. ATR spectra of montmorillonite, saponite, and their respective porous clay heterostructures (PCHs).

© 2022 The Authors. Advanced Sustainable Systems published by Wiley-VCH GmbH

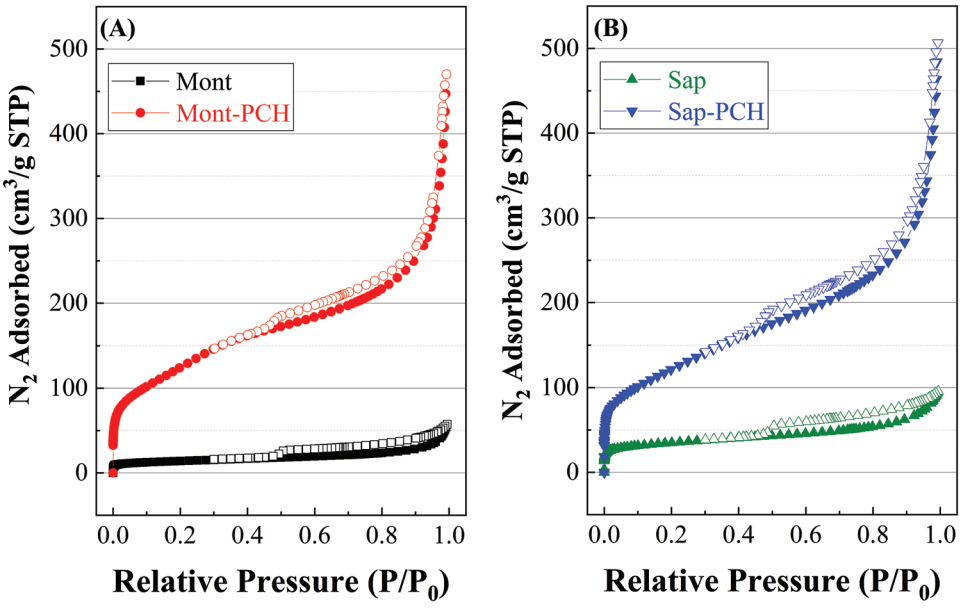

Figure 4. N_2 adsorption–desorption isotherms at –196 °C of A) Mont, Mont-PCH and B) Sap, Sap-PCH.

PCHs, probably due to the calcination of the template diminishes the number of silanol groups, so the hydrophilic character of PCHs decreases.[35,43]

Textural properties of catalysts were determined by N_2 adsorption–desorption at –196 °C (**Figure 4**). According to the IUPAC classification, the isotherms can be considered as Type II, which is characteristic of materials with micro- and macroporosity.[44] With respect to the hysteresis loop, the isotherms can be adjusted to H3, associated with non-rigid aggregates of plate-shaped particles, such as clay minerals or pillared clays.[44] A detailed analysis of the adsorption–desorption isotherms shows that both Mont-PCH and Sap-PCH adsorb a high amount of N_2 at low relative pressure, which reveals the high microporosity of these materials. In the same way, both PCHs also display a clear increase in the N_2 adsorbed at high relative pressure, so these materials also exhibit high macroporosity, probably due to random shift of the phyllosilicate layers after the insertion of the pillars leading to a delamination of the clay, giving rise to a card house structure, as was described previously by Occelli.[45]

The determination of the specific surface area by the Brunauer–Emmett–Teller (BET) method [46] (**Table 2**) confirms an increase in values for both PCHs, being 460 and 445 $m^2\ g^{-1}$ for Mont-PCH and Sap-PCH, respectively. This increase could be mainly attributed to the microporosity, as can be inferred from *t*-plot and V_{MICROP} data (Table 2).[47]

The analysis of the pore size distribution was carried out by the density functional theory (DFT) method (**Figure 5**).[48] Both PCHs show a narrow distribution, mainly in the case of the Mont-PCH. DFT data reveal the existence of pore sizes of 1.27 and 2.83 nm, enough to allow the access and adsorption of reagents and the desorption of potential products to the active sites in the porous structure. As PCHs show microporosity, the micropore size distribution was also studied by the MP method (**Figure 6**),[49] demonstrating that both Mont-PCH and Sap-PCH also possess pores between 0.50 and 0.75 nm.

Thus, it can be concluded that PCHs have micro-, meso-, and macroporosity, in such a way that these suitable textural properties allow them to be used in catalysis.

The surface chemical nature was evaluated by X-ray photoelectron spectroscopy (XPS) (**Table 3**; Figures S1 and S2, Supporting Information). In Si 2p core level spectra, both clays and PCHs show a contribution located between 102.9 and 103.5 eV, typical of silica.[50] In the same way, it is also noteworthy the presence of a band located about 74.8–75.1 eV in the Al 2p core level spectra and a band about 50.2–50.5 eV in the Mg 2p core level spectra attributed to Al_2O_3 and MgO, respectively.[50] The surface atomic concentration values (Table 3) confirm the XRF and XRD data, with a higher Al content in Mont and higher Mg content in Sap.

The formation of the Mont-PCH and Sap-PCH causes a decrease in the concentration of Mg and Al, while the Si content increases due to the formation of SiO_2–ZrO_2 nanoparticles. In this sense, Zr 3d core level spectra show a new contribution at 182.9 eV assigned to the presence of Zr species in the form of ZrO_2 in the porous structure.[50] The analysis of the O 1s core level spectra exhibits an unique band located about 532.2 eV in Mont and Sap, which is assigned to oxidic species. In these

Table 2. Textural properties of montmorillonite, saponite, and their respective porous clay heterostructures (PCHs).

Sample	S_{BET} [$m^2\ g^{-1}$]	*t*-plot [$m^2\ g^{-1}$]	V_P [$cm^3\ g^{-1}$]	V_{MICROP} [$cm^3\ g^{-1}$]
Mont	50	24	0.052	0.011
Mont-PCH	460	240	0.448	0.123
Sap	124	75	0.112	0.034
Sap-PCH	445	138	0.493	0.070
Mont-U	19	–	0.0428	–
Mont-PCH-U	304	180	0.285	0.084
Sap-U	97	45	0.105	0.022
Sap-PCH-U	256	92	0.289	0.043

© 2022 The Authors. Advanced Sustainable Systems published by Wiley-VCH GmbH

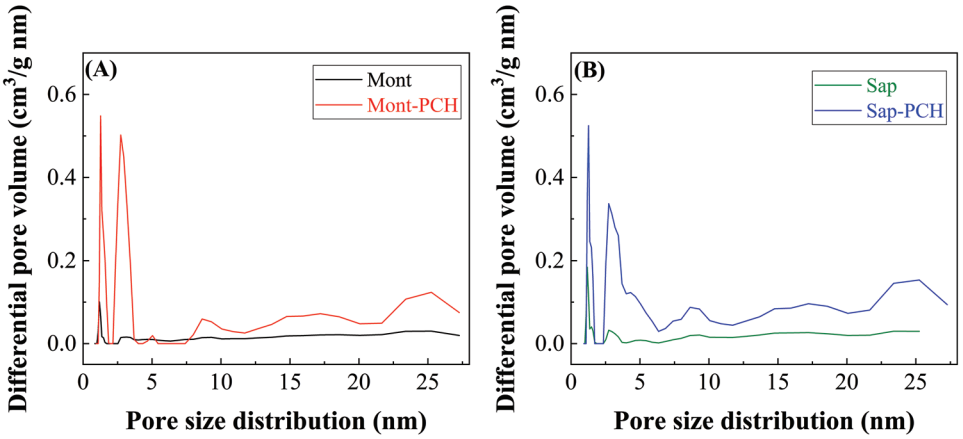

Figure 5. Pore size distribution of A) Mont, Mont-PCH and B) Sap, Sap-PCH estimated by DFT method.

samples, the typical contribution of −OH groups was not observed by XPS, despite ATR data showed the existence of silanol groups (Figure 3). However, both Mont-PCH and Sap-PCH exhibit an additional contribution in the O 1s core level spectra at 530.6 eV, due to the presence of carbonate and/or hydroxyl groups.[50] Finally, C 1s core level spectra show a main signal at 284.8 assigned to the adventitious carbon, while the smaller contributions located about 286.7–286.9 and 289.2–289.4 eV are ascribed to C−O and −O−C=O bonds, respectively.[50]

It has been reported in the literature that one-pot reaction from FUR to GVL takes place through consecutive reactions where Lewis and Brönsted acid sites are involved.[27] Traditionally, the amount of acid sites is determined from NH_3 temperature-programmed desorption (NH_3-TPD), but this does not allow to discern between Lewis and Brönsted acid sites. Moreover, NH_3 is a molecule smaller than FUR, so all the sites estimated from NH_3-TPD are not really available for FUR molecules, mainly considering that clays and mainly PCHs have a high microporosity. Thus, it is necessary to search other probe molecules with dimensions closer to reactants and products.

Considering these premises, the analysis of the acidity was carried out by temperature-desorption of pyridine (pyr) and 2,6-dimethylpyridine (2,6-dmpyr), since pyridine adsorption allows to quantify the total amount of acid sites,[51] while the thermodesorption of 2,6-dimethylpyridine is used as a proton specific probe molecule to estimate the amount of Brönsted acid sites, since the methyl groups have a steric effect in such a way that the access to Lewis acid sites is hindered.[52,53] Thus, the total amount of acid sites in raw clays is relatively low (0.28 and 0.23 mmol pyr g^{-1} for Mont and Sap, respectively) (**Table 4**). The insertion of SiO_2–ZrO_2 pillars to form PCHs increases the acidity, attaining 0.62 and 0.48 mmol pyr g for Mont-PCH and Sap-PCH, respectively, in agreement with data reported in the literature.[34,35] Therefore, Al-rich smectite (montmorillonite) and its respective PCH possess higher acidity than saponite-based samples, confirming that dioctahedral clays display higher acidity than trioctahedral ones.[54] Concerning Brönsted acidity, as determined from 2,6-dimethylpyridine temperature-programmed desorption, the amount of Brönsted acid sites is relatively low in comparison to the total amount of acid sites, being in all cases lower than 0.09 mmol 2,6-dmpyr g^{-1}. This implies that most acid sites can be assigned to Lewis acid sites, which are required for the initial stage of the one-pot process, where FUR is reduced to FOL through CTH.[27] The decrease in the amount of Brönsted acid sites must be ascribed to the dehydroxylation during the calcination of PCHs.

2.2. Catalytic Tests

Raw clays and their corresponding PCHs were evaluated in the CTH of FUR using 2-propanol as sacrificing alcohol (H-donor).

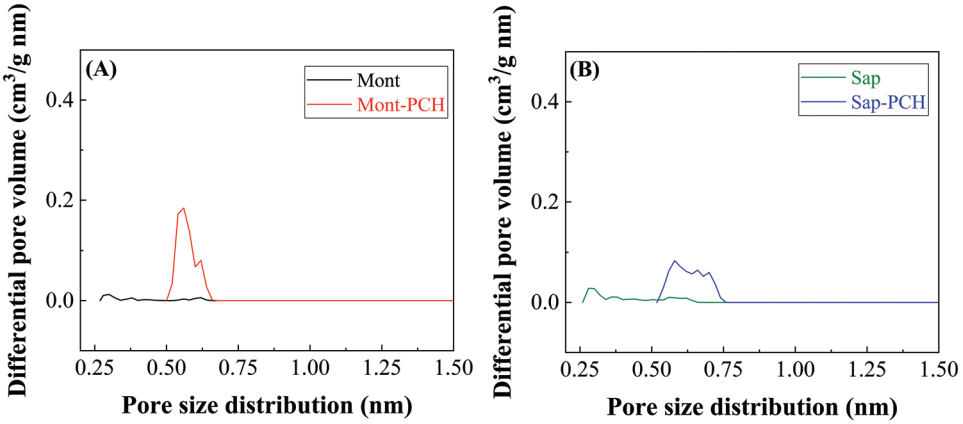

Figure 6. Pore size distribution of A) Mont, Mont-PCH and B) Sap, Sap-PCH estimated by MP method.

© 2022 The Authors. Advanced Sustainable Systems published by Wiley-VCH GmbH

Table 3. XPS data of montmorillonite, saponite, and their respective porous clay heterostructures (PCHs).

Sample	Surface atomic concentration, %/(binding energy, eV)								
	C 1s	O 1s	Si 2p	Zr 3d	Al 2p	Mg 2p	Fe 2p	Na 1s	Ca 2p
Mont	6.50 (284.8) 0.73 (286.8) 0.36 (289.4)	61.87 (532.2)	18.71 (102.9)	–	6.16 (74.8)	2.18 (50.3)	0.99 (712.8)	1.92 (1072.5)	0.58 (351.4)
Mont-PCH	7.28 (284.8) 1.17 (286.9) 0.57 (289.3)	60.50 (532.7) 3.36 (530.6)	22.86 (103.2)	1.67 (182.9)	1.98 (75.1)	0.18 (50.4)	0.42 (712.6)	–	–
Sap	9.19 (284.8) 1.23 (286.7) 0.77 (289.4)	57.07 (532.0)	16.53 (103.0)	–	1.85 (74.4)	10.19 (50.2)		2.80 (1072.4)	–
Sap-PCH	9.89 (284.8) 1.19 (286.9) 0.35 (289.2)	57.11 (532.7) 5.01 (530.6)	21.86 (103.5)	2.42 (182.9)	0.51 (74.7)	1.66 (50.5)	–	–	–
Mont-U	17.78 (284.8) 2.55 (286.7) 0.76 (288.5)	54.25 (532.0)	15.35 (102.7)	–	5.16 (74.6)	1.68 (50.4)	0.99 (712.5)	0.77 (1072.3)	0.71 (351.5)
Mont-PCH-U	19.48 (284.8) 3.55 (286.6) 0.77 (288.7)	54.34 50.63 (532.8) 3.71 (530.7)	18.95 (103.4)	1.99 (103.0)	0.61 (74.5)	0.05 (50.4)	0.25 (712.6)	–	–
Sap-U	11.87 (284.8) 1.95 (286.7) 0.35 (288.7)	57.31 (532.1)	16.40 (103.1)	–	1.87 (74.6)	9.15 (50.4)	0.45 (712.4)	0.66 (1072.5)	–
Sap-PCH-U	15.83 (284.8) 3.49 (286.4) 0.50 (288.5)	51.81 (532.8) 4.90 (530.5)	19.92 (103.3)	2.51 (182.8)	0.32 (74.7)	0.68 (50.2)	–	–	–

In a preliminary study, among several phyllosilicates (kaolinite, montmorillonite, saponite, palygorskite, sepiolite, and ripidolite) studied in this reaction at 170 °C for 3 h, both smectites (Mont and Sap) reached the highest conversion values (**Figure 7**), 74% and 79%, respectively. The TOT sheets of montmorillonite and saponite are more prone to host molecules, like FUR, in their interlayer region, than the fibrous structures of sepiolite or palygorskite, with a high proportion of microcavities.[34]

Regarding the selectivity pattern, Sap, with a lower acidity, gives rise to FOL as single product with a yield of 41%, whereas Mont, besides FOL as main product, leads to i-propyl furfuryl ether (iPFE) and i-propyl levulinate (iPL), though in minor proportions (**Scheme 1**). The use of a catalyst with a higher

© 2022 The Authors. Advanced Sustainable Systems published by Wiley-VCH GmbH

Table 4. Acidity determined from pyridine-(Pyr-TPD) and 2,6-dimethylpyridine-(2,6-DMPyr-TPD) temperature-programmed desorption studies.

Sample	Pyr-TPD [mmol g^{-1}]	2,6-DMPyr-TPD [mmol g^{-1}]	(Pyr-TPD-2,6)–(DMPyr-TPD) [mmol g^{-1}]
Mont	0.28	0.06	0.22
Mont-PCH	0.62	0.04	0.58
Sap	0.23	0.09	0.14
Sap-PCH	0.48	0.05	0.43

acidity, together with the coexistence of Lewis and Brönsted acid sites, favors the existence of consecutive reactions, such as the etherification of FOL and the opening of the furan ring by a hydration reaction (Scheme 1). In this sense, previous studies have reported that the etherification FOL → iPFE takes places through Lewis and/or Brönsted acid sites, while the hydration and ring opening reaction (iPFE → iPL) proceeds via Brönsted acid sites.[55] In both cases, it is noteworthy the formation of a high amount of undetected products, which could be explained by the polymerization of FUR, or FOL, on acid sites, as inferred from the darker coloration the reaction medium.[29]

Previous studies have demonstrated that the one-pot process from FUR to GVL takes usually place with Zr-based catalysts.[28–32] Thus, the insertion of SiO_2–ZrO_2 nanoparticles between adjacent layers of Mont and Sap allows to improve textural and acid properties (Figures 4–6 and Tables 2 and 4) and could provide active catalysts for these one-pot reactions.

The reaction temperature (**Figure 8**) affects FUR conversion, which raises with the temperature. In the case of Mont and Sap, the conversion (Figure 8A) increases from 3% and 8%, after 3 h, at 90 °C, up to 64% and 78%, respectively, at 170 °C. This improvement of FUR conversion with the temperature is more pronounced after the insertion of SiO_2–ZrO_2 pillars nanoparticles, attaining conversion values of 95% and 100% for Mont-PCH and Sap-PCH, respectively, after 3 h of reaction at 170 °C.

Regarding the reaction products (Figure 8B–F), a wide range of products, whose proportion depends on the reaction temperature, can be detected. In the case of Mont and Sap, the one-pot process is stopped in earlier steps, obtaining FOL and iPFE as main products. It is well known that the reduction of FUR to FOL takes place by the CTH reactions through a six-member intermediate, requiring Lewis acid sites and 2-propanol as hydrogen donor,[56] reaching FOL yields of 41% and 36% for Sap and Mont, respectively, after 3 h at 170 °C. In the same reaction, as FUR is reduced to FOL, 2-propanol, used as a sacrificial alcohol in the reaction, is oxidized simultaneously to acetone.

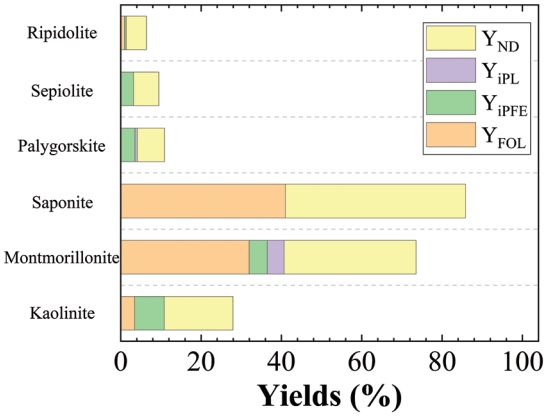

Figure 7. Conversion and yield patterns of several raw clays in the one-pot process from FUR. (Experimental conditions: reaction temperature: 170 °C, reaction time: 3 h, i-Pr-OH/FUR molar ratio: 50, 0.1 g of catalyst, FUR/catalyst weight ratio: 1).

Moreover, the raw clay with the highest acidity (Mont) also favors the etherification reaction with the sacrificing alcohol, attaining an iPFE yield of 16%, after 3 h at 150 °C. This etherification reaction (FOL → iPFE) can take place through Brönsted and Lewis acid sites,[56] and, in this sense, increasing Lewis acidity (Table 4) seems to favor this etherification reaction.

In the case of Mont-PCH and Sap-PCH (Figure 8), the higher FUR conversion is accompanied by the formation of more advanced products in the one-pot process from FUR to GVL, so the presence of SiO_2–ZrO_2 nanoparticles, as well as the improvement of textural and acid properties, improve the catalytic performance. Thus, both FOL and iPFE are mainly obtained at lower temperatures. In addition, PCH of Al-rich smectites (Mont-PCH) is more selective to iPFE, while that derived from Mg-rich smectites (Sap-PCH) requires higher temperatures to attain higher iPFE yields (35% after 3 h at 130 °C). From these data, it can be inferred that the presence of Mg species seems to favor the CTH of FUR to FOL and its subsequent etherification to iPFE.

The increase in the reaction temperature decreases both FOL and iPFE yields, but concomitantly increases the iPL yield through a rehydration reaction, via furan ring opening, in the presence of Brönsted acid sites.[56,57] The acidity study has revealed that the proportion of Brönsted acid sites, ascribed to the remaining silanol groups, is relatively low (Table 4), although this seems to be enough for the conversion of FOL and iPFE into iPL. It has been previously reported that the amount of Brönsted acid sites must be modulated, since its excess could cause uncontrolled side reactions leading to soluble and insoluble (humins) polymers.[56] Thus, Mont-PCH and Sap-PCH attain iPL yields of 33 and 28%, respectively, after 3 h at 170 °C

In the next step of the one-pot process, iPL would react with the sacrificing alcohol (2-propanol) through Lewis acid sites to form i-propyl 4-hydroxy pentanoate.[56] However, this product was not observed in any case, so it is expected that once i-propyl 4-hydroxy pentanoate is obtained, this suffers an intramolecular lactonization, which implies a cyclation, to form GVL through both Brönsted and Lewis acid sites (Scheme 1).[56,57] This product is only obtained with both PCHs at high temperature, attaining GVL yields of 14% and 11% for Mont-PCH and Sap-PCH, respectively, after 3 h at 170 °C. These data agree with the literature, since previous papers have reported that the presence of Zr species in porous silicas, or zeolites, favors the formation of GVL, although the lactonization reaction requires long reaction times and high reaction temperature in comparison to other reactions of the one-pot process.[29,56,58,59]

Finally, the amount of undetected products increases with the reaction temperature, obtaining a yield close to 40%, after 3 h at 170 °C. In this sense, it should be noted that both FUR and FOL are highly reactive molecules, and they can react with themselves, mainly when the reaction temperature increases, leading to the formation of humins, which are deposited on the surface of the catalyst, as was observed by XPS in the used catalysts (Table 3).

© 2022 The Authors. Advanced Sustainable Systems published by Wiley-VCH GmbH

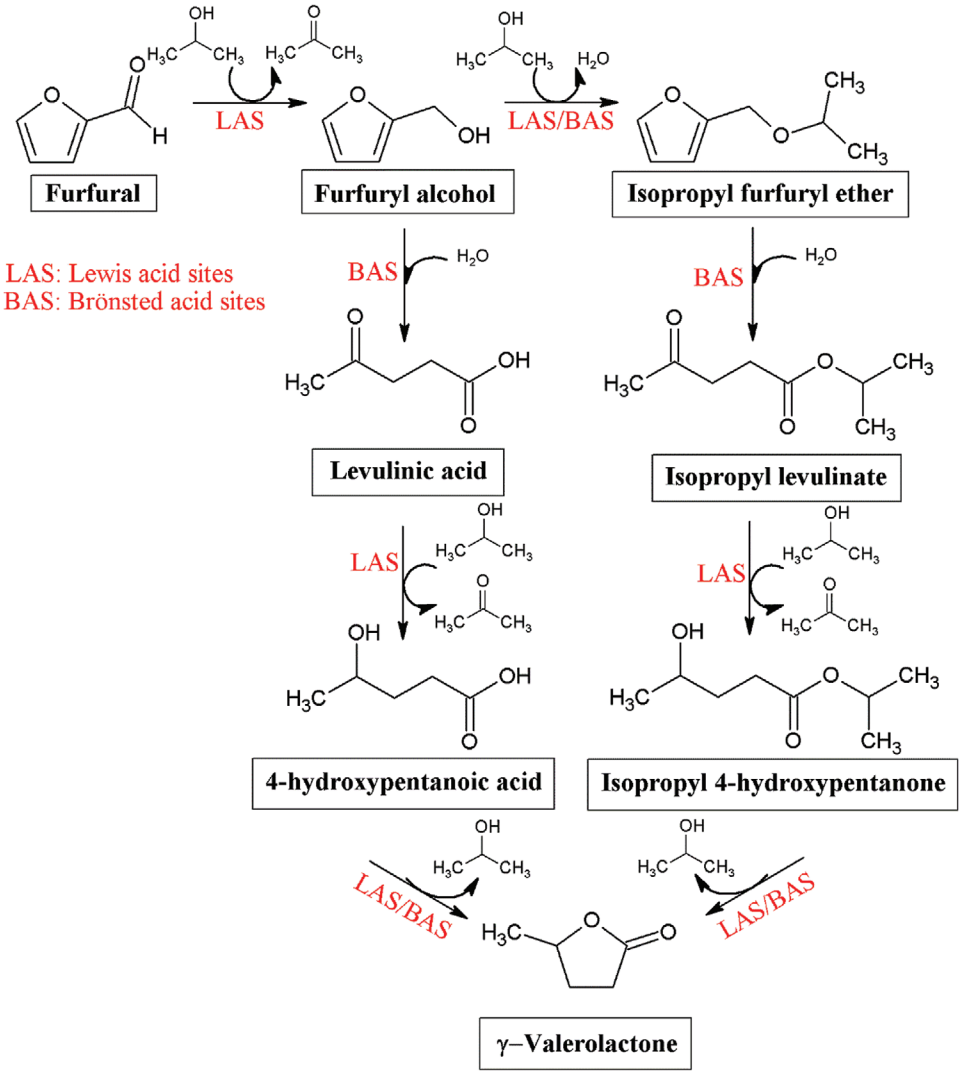

Scheme 1. Mechanism of the FUR valorization in one-pot reaction.

As both PCHs with SiO_2–ZrO_2 pillars reached the highest conversion values, they were selected to carry out a kinetic study at 170 °C (**Figure 9**). As expected, the FUR conversion increases with the reaction time, obtaining an almost full conversion after only 1.5 h for both PCHs. Despite these catalysts display total conversion from 1.5 h of reaction, the selectivity pattern varies with the reaction time, which suggests the existence of consecutive reactions to give rise to GVL. Regarding the obtained products, FOL and iPFE are obtained at shorter reaction times, so both the CTH reaction and the etherification of FOL with 2-propanol occur relatively fast. Moreover, Mont-PCH reaches a maximum FOL yield of 31% after 1.5 h, and a maximum iPFE yield of 32% after only 22 min. Both FOL and iPFE yields decay after longer reaction time, mainly in the case of iPFE, which is not detected after only 1.5 h. In the case of the Sap-PCH, a similar trend is observed, although the highest FOL yield is slightly lower than that attained with Mont-PCH catalyst (15% after 1.5 h), while the maximum iPFE yield is slightly higher, although a longer reaction time is required to obtain the maximum of this product (37% after 3 h). In addition, the total disappearance of iPFE to form other products requires a longer reaction time, as was observed in the test where the reaction temperature was modified (Figure 8).

The decrease in FOL and iPFE yields along the reaction time is accompanied by the formation of iPL, which is faster in the case of Mont-PCH (50% after 1.5 h of reaction), while the formation of iPL in Sap-PCH is more gradual, since the highest iPL yield is 39% after 12 h. This fact could be ascribed to the existence of a higher proportion of acid sites in the case of Mont-PCH, although the opening ring takes place on Brönsted acid sites. This type of acid sites is minority and similar in Mont-PCH and Sap-PCH; however, this amount seems to be enough for the formation of iPL. The use of an excess of Brönsted acid sites can lead to undesired side reactions, as previously noted.[56]

The use of a longer reaction time favors the CTH and subsequent lactonization of iPL to GVL. In the case of Mont-PCH, a higher GVL yield is observed in comparison to Sap-PCH, probably due to its higher proportion of acid sites; in any case, both catalysts reach a GVL yield close to 27% after 24 h.

© 2022 The Authors. Advanced Sustainable Systems published by Wiley-VCH GmbH

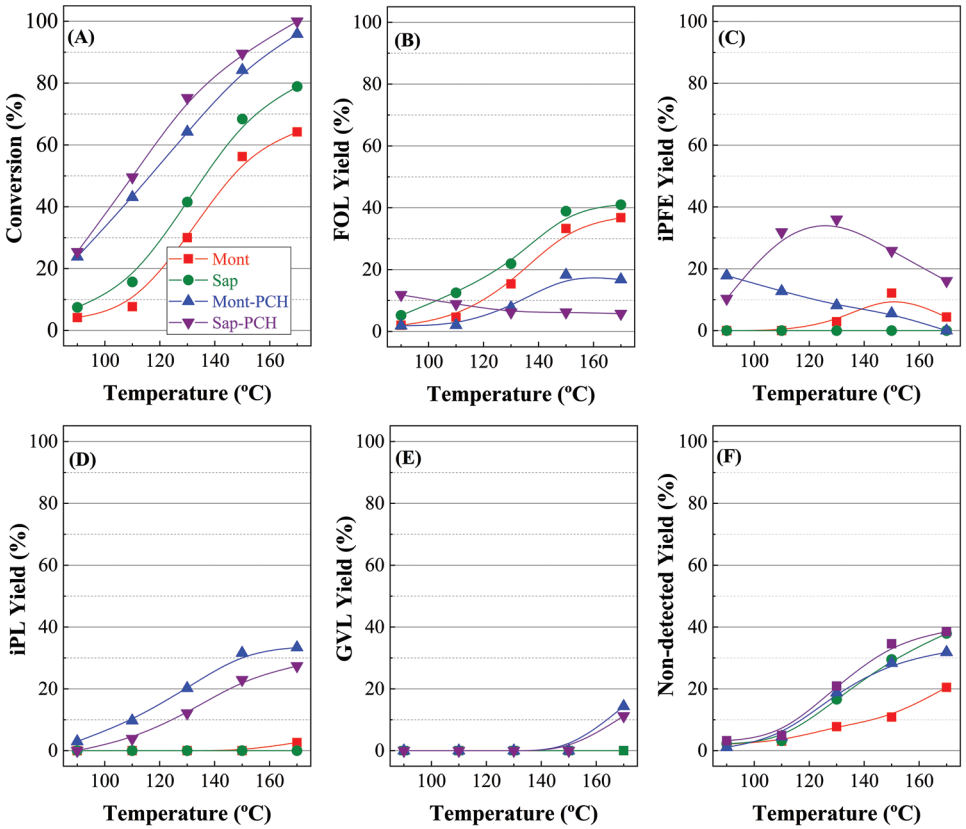

Figure 8. A) FUR conversion, B) FOL yield, C) IpFE yield, D) IpL yield, E) GVL yield, and F) nondetected product yield in the one-pot reaction of FUR into valuable products using Mont, Mont-PCH, Sap, and Sap-PCH as catalysts. (Experimental conditions: temperature reaction: 90–170 °C, reaction time: 3 h, i-Pr-OH/FUR molar ratio: 50, 0.1 g of catalyst, FUR/catalyst weight ratio: 1).

Finally, as expected, a longer reaction time leads to a darker reaction solution, which causes an increase in the proportion of undetected products, reaching yields close to 50%. These data also reveal that the higher proportion of undetected products appear at short reaction time (between 35% and 40% of nondetected products after 3 h). These data suggest that the reagent, i.e., FUR, as well as the initial products of the one-pot process (FOL and iPFE) must be the main compounds involved in catalytic deactivation. In this sense, it has been reported in the literature that FUR and FOL are prone to suffer polymerization reactions in the presence of acid sites.[60] This agrees with the obtained data by XPS (Table 3), since the catalyst with higher acidity also displays a higher proportion of carbonaceous species on the catalyst surface.

A key parameter in heterogeneous catalysts is the ability to recuperate catalysts to be used for several cycles. Thus, both Mont-PCH and Sap-PCH were tested for 3 h at 170 °C and reused during 4 cycles (**Figure 10**). Between each cycle the catalyst was washed with 2-propanol and dried. The catalytic results show a full conversion in all tests, except for the fourth cycle for Sap-PCH catalyst, where FUR conversion slightly decreases until 95%. However, the selectivity pattern changes with the number of cycles. Thus, the GVL yield progressively decreases with the number of cycles, disappearing in the case of Mont-PCH and diminishing up to 4% for Sap-PCH. This decline coincides with an increase in iPL yield, mainly after the second cycle, although this product also declines in subsequent cycles from 37% to 25% in the case of Mont-PCH and from 37% to 24% for Sap-PCH. The decrease in GVL and iPL after several cycles is accompanied by an increase in FOL in the case of Mont-PCH, reaching a yield of 44% after fourth cycle, while in Sap-PCH causes a rise in FOL (16% after the fourth cycle) and iPFE (43% after the fourth cycle) yield. In addition, it is also noteworthy that the amount of undetected product also decreases with the number of cycles, being 22% for Mont-PCH and 13% for Sap-PCH after the fourth cycle. From these data, it can be concluded that both catalysts are progressively deactivated, in such a way that, despite these catalysts show a full or almost full conversion, the one-pot reaction is retained in earlier stages as the number of cycles progresses. The regeneration of Mont-PCH and Sap-PCH by calcination at 600 °C leads to a similar selectivity pattern to that observed after the first cycle, although slight modifications are observed. This temperature was selected for removing the carbonaceous deposits, according to the TGA analysis.[61] After calcination, the amount of FOL, iPFL, and iPL increase, while the levels of GVL and nondetected products slightly decrease. Therefore, the calcination favors the formation of those products that are obtained in earlier steps of the one-pot process. This suggests that the calcination reaction can cause a decrease in the amount of acid sites, thus hindering the progress of the one-pot process, i.e., the formation of GVL is slightly disfavored. On the other hand,

© 2022 The Authors. Advanced Sustainable Systems published by Wiley-VCH GmbH

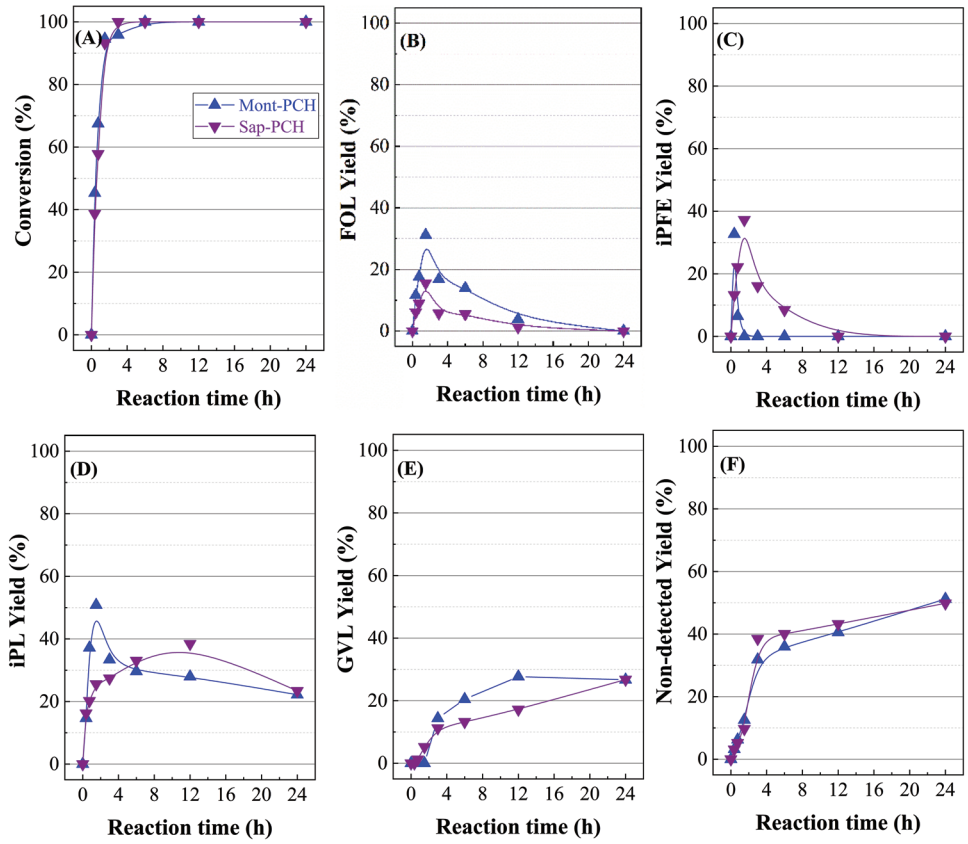

Figure 9. A) FUR conversion, B) FOL yield, C) IpFE yield, D) IpL yield, E) GVL yield, and F) nondetected product yield in the one-pot reaction of FUR into valuable products using Mont-PCH and Sap-PCH as catalysts. (Experimental conditions: 0.1 g of catalyst, temperature reaction: 170 °C, reaction time: 0–24 h, i-Pr-OH/FUR molar ratio: 50, FUR/catalyst weight ratio: 1).

the presence of a lower amount of acid sites could also minimize the polymerization of FUR or FOL to form undetected polymeric products.

In order to understand the changes in the selectivity pattern when the catalysts have been reused for several cycles, the used catalysts were recovered after the reaction at 170 °C for 24 h to be characterized.

The analysis of textural properties of the used catalysts (Table 2) evidences the worsening of specific surface area and pore volume values. The analysis of the adsorption–desorption isotherms (Figures S3 and S4, Supporting Information) confirms a clear decrease in the micro- and mesoporosity of catalysts, which must also imply a decrease in the amount of available active sites and, consequently, a decrease in catalytic activity, hindering that the one-pot process from FUR to GVL goes further, being retained in earlier stages (Figure 10).

To understand the worsening of textural properties, the used catalysts were also characterized by XPS (Table 3; Figures S1 and S2, Supporting Information). The analysis of the surface chemical composition of used catalysts shows an

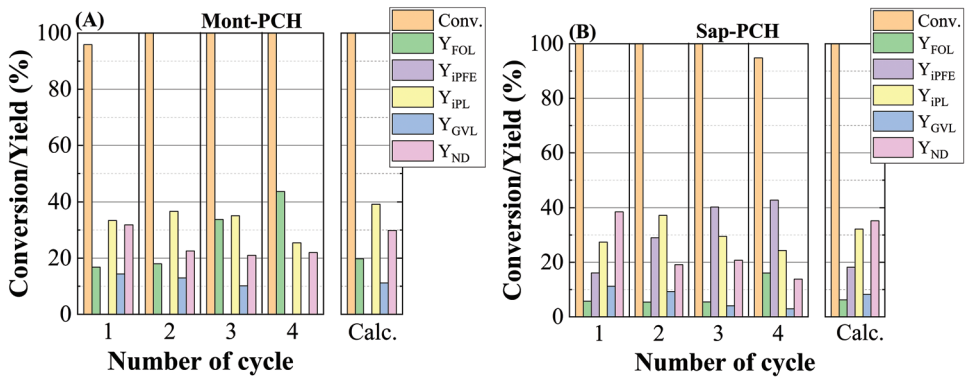

Figure 10. Reuse of the Mont-PCH and Sap-PCH for four cycles and a final calcination. (Experimental conditions: temperature reaction: 170 °C, reaction time: 3 h, i-Pr-OH/FUR molar ratio: 50, 0.1 g of catalyst, FUR/catalyst weight ratio: 1).

© 2022 The Authors. Advanced Sustainable Systems published by Wiley-VCH GmbH

increase in the carbon content in all cases (raw clays and their respective PCHs). This fact suggests the formation of carbonaceous deposits on the catalyst surface, which would be probably blocking both Lewis and Brönsted acid sites involved in the one-pot process. In this sense, previous authors have reported that the strong interaction of FUR and/or FOL with the active sites would favor their polymerization.[16] In addition, the alcohol used as hydrogen donor can be deprotononated, forming alkoxydes, which tend to interact strongly with the active sites involved in the CTH processes.[62]

In an additional test, the analysis of each step in the reaction was carried out to confirm the proposed mechanism (**Figure 11**). The catalytic tests, performed at 110 °C for 6 h (Figure 11A), show the high conversion of FUR to iPFE in Mont-PCH and Sap-PCH, indicating that the CTH reaction to form FOL and its subsequent etherification takes place at a relatively low temperature.[23,58] In addition, both catalysts also yield iPL, although this appears in major proportion in the case of Mont-PCH, probably due to its higher acidity, in such a way that the furan ring opening can occur at low temperature, although requiring longer reaction time to reach a high conversion. On the other hand, it is also noteworthy that both catalysts give rise to a high proportion of undetected products, whose yields are 20% and 15% for Mont-PCH and Sap-PCH, respectively.

If the reaction starts from FOL, in the presence of PCH catalysts, both conversion and yields toward iPFE and iPL slightly increase, as well as the proportion of undetected products. This could be expected, since FOL is a more reactive molecule than FUR.

The study of reaction starting from iPL shows a lower conversion, with values below 8%. In no case were previously identified products detected, so these conversion values were assigned to undetected products, although to a lesser extent than those obtained when the reaction started from FUR of FOL, in such a way that the lactonization reaction to form GVL is the limiting step in the one-pot process, as was previously reported by other authors.[56]

The kinetic study of the reaction was also carried out by analyzing the different steps of the one-pot process at 170 °C (Figure 11B) for comparative purposes. In all cases, the conversion value is higher than that observed at 110 °C, while the selectivity pattern also differs. Thus, when the reaction starts from FUR, it can be observed a total conversion after 4 h of reaction, but the amount of iPFE is lower than that observed at 110 °C. However, the proportion of FOL and iPL is higher in both PCH-based catalysts. From these data, it can be inferred that the CTH reaction from FUR to FOL proceeds faster at higher temperature. Then, FOL suffers the etherification reaction to form iPFE, which evolves fast to iPL in such a way that iPFE is hardly detected to 170 °C in the case of Mont-PCH. Regarding Sap-PCH, this still displays a high iPFE yield, so the use of a Mg-rich smectite, as saponite, in the formation of PCH can favor the etherification reaction. The low proportion of iPFE using Mont-PCH at 170 °C is supported by kinetic studies carried out with Zr-SBA-15 for this same reaction by other authors, who confirmed that the FOL → alkyl furfuryl ether → alkyl levulinate steps were the fastest in the one-pot process of FUR to GVL.[57] The use of a higher temperature also favors the lactonization reaction to obtain GVL, mainly for longer reaction time, confirming that this stage is the limiting step in the one-pot process. On the other hand, it should also be noted that the reaction from FUR at 170 °C gives rise to a greater amount of undetected products due to polymerization processes, mainly from FOL and FUR, which are favored at higher temperatures, reaching nondetected products yields of 35–40% after 6 h of reaction at 170 °C.

If the reaction is carried out from FOL at 170 °C, the total conversion was reached at shorter reaction times, after only 3 h. In the case of Mont-PCH, the formation of iPL and GVL is enhanced, while iPFE decreases and iPL and GVL rise with Sap-PCH. From the selectivity patterns, it can be established that if the reaction starts from FOL, a greater progression can be observed in the one-pot process. Nonetheless, this high reactivity is also accompanied by an increase in the proportion of undetected products.

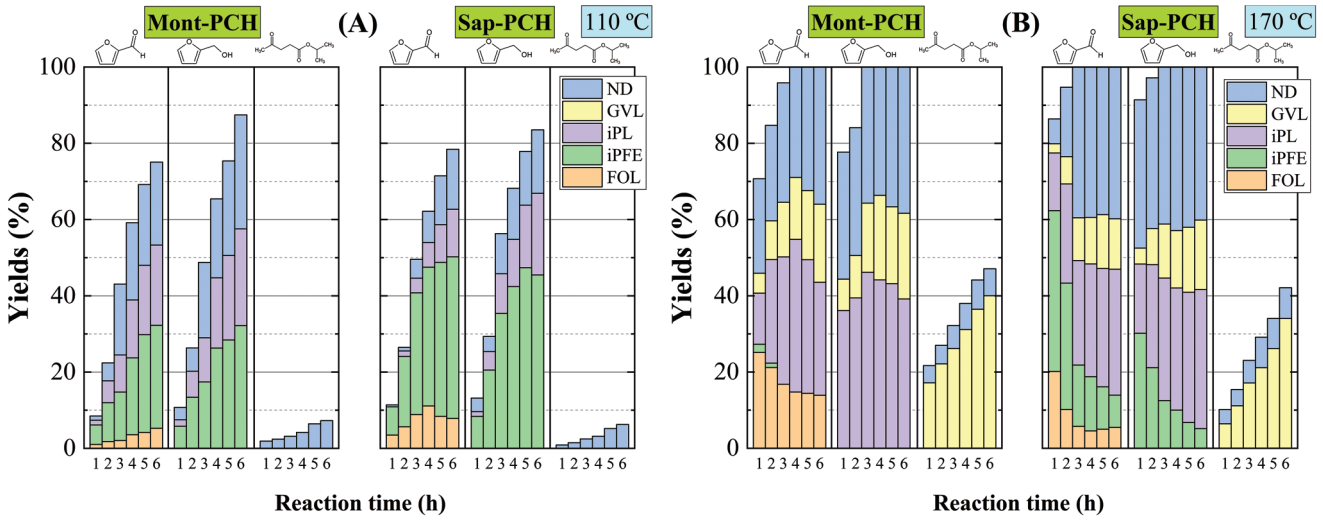

Figure 11. Conversion and yields starting from FUR, FOL, and iPL using Mont-PCH and Sap-PCH as catalysts at A) 110 °C and B) 170 °C. (Experimental conditions: reaction time: 3 h, i-Pr-OH/reactive molar ratio: 50, 0.1 g of catalyst, reactive/catalyst weight ratio: 1).

© 2022 The Authors. Advanced Sustainable Systems published by Wiley-VCH GmbH

Finally, as was observed at 110 °C, the reaction from iPL leads to lower conversion values for both catalysts, corroborating the limiting step of this reaction. However, it can be observed that the reaction from iPL gives rise to the highest GVL yield and a relatively low proportion of undetected products, again confirming that both FUR and FOL must be the main molecules involved in the formation of soluble and insoluble polymers in the one-pot process.

3. Conclusions

Several phyllosilicates have been tested in the valorization of FUR through a one-pot process. Between them, two smectites (Mont and Sap) showed the highest catalytic activity, obtaining FOL and iPFE as main products. To enhance their catalytic activity, these smectites were pillared by the insertion of SiO_2–ZrO_2 nanoparticles in their interlayer region, forming PCHs, which improve the textural and acid properties. This latter is due to the presence of ZrO_2, which provides Lewis acid sites involved in hydrogen catalytic transfer to reduce an aldehyde or ketone into alcohols. In addition, the small proportion of Brönsted acid sites also promotes dehydration or furan ring opening reactions.

The synthesis of these PCHs significantly improves catalytic activity, obtaining almost full FUR conversion at 170 °C, after 3 h of reaction. On the other hand, the reaction temperature plays an important role in determining the selectivity pattern, since a lower reaction temperature (110 °C) fosters the formation of FOL and iPFE, that is, the reaction is retained in the first steps of the one-pot process. However, a higher reaction temperature (170 °C) promotes consecutive reactions by the coexistence of Lewis and Brönsted acid sites. Thus, the amounts of iPL and GVL increase, mainly at longer reaction times. The analysis of the catalytic activity from several intermediate products of the one-pot process reveals that the lactonization reaction is the limiting step, being only favored at high temperature (170 °C) and longer reaction time.

The reusing study showed an almost full conversion with both PCHs, although the selectivity pattern slightly differs according to the number of cycles increases. Thus, the proportions of GVL and iPL decrease, while FOL and iPFE increase. This means that the reaction is retained in intermediate steps of the one-pot process, as a consequence of the formation of carbonaceous deposits due to the polymerization of FUR and/or FOL, leading to soluble and insoluble polymers, in such a way that Brönsted and Lewis sites are partially blocked.

4. Experimental Section

Catalyst Synthesis: A montmorillonite and a saponite were selected as starting materials to be evaluated in FUR valorization through cascade (one-pot) reactions. These materials were used without prior purification treatment.

The synthesis of PCHs, from montmorillonite and saponite, was carried following the methodology described by Cecilia et al. [35,36] In both cases, 2.5 g of raw clay were suspended in 100 mL of 1-propanol. Then, 9 g of hexadecyltrimethylammonium bromide (HDTMABr) were added to this suspension to favor a cationic exchange of the alkaline cations by a bulkier organic cation, in such a way swelling of the interlaminar space takes place. After 48 h, the gel was filtered and washed until neutral pH to remove the non-adsorbed bulky cation in the clay mineral. In the next step, the gel was resuspended in 250 mL of H_2O and stirred for 24 h. After that, 0.9 g dodecylamine were dissolved into 25 mL of 1-propanol and added to the mother solution, and stirred for 24 h. In the last step, 0.05 mol of a solution of tetraethyl orthosilicate and zirconium propoxide with a Si/Zr molar ratio of 5 was dissolved in 15 mL of 1-propanol, added to the suspension, and stirred for 48 h.

Finally, solids were filtered and washed with water, dried for 12 h at 80 °C and calcined at 550 °C with a rate of 1 °C min^{-1}, maintaining this temperature for 6 h, to remove the organic matter. The catalysts were labeled as Mont and Sap for the raw montmorillonite and saponite, respectively, while the label of Mont-PCH and Sap-PCH is assigned to their respective PCHs, which have Si/Zr nanoparticle with a molar ratio of 5.

Characterization of Catalysts: The crystallinity and the mineralogical content of the raw clays and their respective PCHs were determined by X-ray diffraction. These experiments were performed in a PANalytical X'Pert PRO equipment, using a germanium monochromator, the Cu Kα (1.5406 Å) radiation. The diffractograms were carried out over a 2θ range of 2°–65° with Bragg-Brentano geometry and a step size of 0.017°.

Elemental composition was determined with a wavelength disperse X-ray fluorescence spectrometer (ARL ADVANTXP) and a UNIQUANT software, with the X-ray tube set at 60 kV.

The morphology was determined by TEM in an FEI Thalos F200X equipment supplied by Thermo Fisher Scientific). This equipment combines outstanding high-resolution STEM and TEM imaging. The samples were dispersed in ethanol and a drop of the suspension was put on a Cu-grid (300 mesh).

ATR spectra were performed in a Vertex70 FT-IR spectrophotometer model supplied by Bruker, acquiring the spectra with a spectral resolution of 4 cm^{-1} and a number of accumulations of 64, between 4000 and 500 cm^{-1}.

Textural properties were determined from their N_2 adsorption–desorption isotherms at –196 °C, using an ASAP 2020 Micromeritics equipment. In a preliminary step, samples were outgassed at 200 °C and a pressure of 10^{-4} mbar overnight. The specific surface area was determined by the BET method, with a N_2 molecule cross-section of 16.2 $Å^2$. The pore size and micropore size distributions were determined by DFT[48] and MP method, [49] respectively.

The surface chemical composition was estimated by XPS, using a Physical Electronics PHI 5700 spectrometer with non-monochromatic Mg Kα radiation (300 W, 15 kV, 1253.6 eV) with a multichannel detector. The spectra were recorded in the constant-pass energy mode at 29.35 eV with a 720 µm diameter analysis area. Charge referencing was measured against adventitious carbon (C 1s at binding energy (BE) of 284.8 eV). The PHI ACCESS ESCA-V 6.0F software package was used for the acquisition and data analysis, whereas a Shirley-type background was subtracted from the signals. All the recorded spectra were fitted with Gaussian–Lorentzian curves to determine more accurately the BE of different element core levels.

The acidity of catalysts was evaluated by adsorption–desorption of pyridine (pyr) and 2,6-dimethylpyridine (dmpyr) at 100 °C, by using a thermogravimetric system (CI Electronics) and 25 mg of dry catalysts. Prior to the pyridine or 2,6-dimethylpyridine adsorption started, samples were degassed at 150 °C for 2 h. For the adsorption experiments, an inlet partial pressure of pyr or dmpyr of 0.02 atm was used. This partial pressure was established by saturating 150 mL min^{-1} of N_2 with the corresponding organic base in a saturator at a determined temperature. Once the sample was saturated with pyr or dmpyr, desorption was carried out at 100 °C, by using a N_2 flow of 150 mL min^{-1}. The total amount of pyr or dmpyr chemisorbed was calculated from the final weight of the sample.

Catalytic Tests: The one-pot process to valorize FUR was carried out in glass reactors (Ace, 15 mL) supplied by Merck. In a typical experiment, 100 mg of catalyst were mixed with 0.1 mmol of FUR dissolved in 2-propanol, used as sacrificing alcohol, maintaining a 2-propanol:FUR

© 2022 The Authors. Advanced Sustainable Systems published by Wiley-VCH GmbH

molar ratio of 50, and 0.02 mL of o-xylene used as internal standard. Prior to each experiment, the reactors were always purged with helium. Reaction time was extended until 24 h, under continuous stirring (300 rpm), whereas the reaction temperature ranged between 90 and 170 °C. The temperature was controlled by a thermocouple directly in contact with an aluminum block. After finishing the reaction time, the reactor was moved away from the aluminum block and cooled in a water bath. Samples were microfiltered and analyzed by a gas chromatography (Shimadzu GC-14A), equipped with a Flame Ionization Detector and a CP-Wax 52 CB capillary column. The furfural conversion and yield were calculated as follows

$$\text{Conversion}\,(\%) = \frac{\text{mol of furfural converted}}{\text{mol of furfural fed}} \times 100 \quad (1)$$

$$\text{Yield}\,(\%) = \frac{\text{mol of product}}{\text{mol of furfural fed}} \times 100 \quad (2)$$

Supporting Information

Supporting Information is available from the Wiley Online Library or from the author.

Acknowledgements

The authors are grateful for financial support from the Spanish Ministry of Science, Innovation and Universities (RTI2018-94918-B-C44 project), FEDER (European Union) funds (UMA18-FEDERJA-171), and the University of Malaga. C.P.J.-G. and C.G.-S. acknowledge Junta de Andalucía and FEDER funds, respectively, for their postdoctoral contracts. Funding for open access charge: Universidad de Málaga/CBUA.

Conflict of Interest

The authors declare no conflict of interest.

Data Availability Statement

The data that support the findings of this study are available from the corresponding author upon reasonable request.

Keywords

furfural, one-pot processes, porous clay heterostructures, smectites, γ-valerolactone

Received: November 16, 2021
Revised: January 26, 2022
Published online:

[1] K. Sanderson, *Nature* **2011**, *474*, S12.
[2] H. P. Vu, L. N. Nguyen, M. T. Vu, M. A. H. Johir, R. McLaughlan, L. D. Nghiem, *Sci. Total Environ.* **2020**, *743*, 140630.
[3] A. K. Kumar, S. Sharma, *Bioresour. Bioprocess.* **2017**, *4*, 7.
[4] A. S. Mamman, J. M. Lee, Y. C. Kim, I. T. Hwang, N. J. Park, Y. K. Hwang, J. S. Chang, J. S. Hwang, *Biofuels, Bioprod. Biorefin.* **2008**, *2*, 438.
[5] R. Mariscal, P. Maireles-Torres, M. Ojeda, I. Sádaba, M. L. Granados, *Energy Environ. Sci.* **2016**, *9*, 1144.
[6] P. L. Arias, J. A. Cecilia, I. Gandarias, J. Iglesias, M. López Granados, R. Mariscal, G. Morales, R. Moreno-Tost, P. Maireles-Torres, *Catal. Sci. Technol.* **2020**, *10*, 2721.
[7] Y. Wang, D. Zhao, D. Rodríguez-Padrón, C. Len, *Catalysts* **2019**, *9*, 796.
[8] A. Mandalika, L. Qin, T. K. Sato, T. Runge, *Green Chem.* **2014**, *16*, 2480.
[9] K. Yan, G. Wu, T. Lafleur, C. Jarvis, *Renewable Sustainable Energy Rev.* **2014**, *38*, 663.
[10] D. Hu, H. Xu, Z. Yi, Z. Chen, C. Ye, Z. Wu, H. F. Garces, K. Yan, *ACS Sustainable Chem. Eng.* **2019**, *7*, 15339.
[11] B. Liu, S. Xu, M. Zhang, X. Li, D. Decarolis, Y. Liu, Y. Wang, E. K. Gibson, C. R. A. Catlow, K. Yan, *Green Chem.* **2021**, *23*, 4034.
[12] G. Chuah, S. Jaenicke, Y. Zhu, S. Liu, *Curr. Org. Chem.* **2006**, *10*, 1639.
[13] R. López-Asensio, J. A. Cecilia, C. P. Jiménez-Gómez, C. García-Sancho, R. Moreno-Tost, P. Maireles-Torres, *Appl. Catal., A* **2018**, *556*, 1.
[14] C. García-Sancho, C. P. Jiménez-Gómez, N. Viar-Antuñano, J. A. Cecilia, R. Moreno-Tost, J. M. Mérida-Robles, J. Requies, P. Maireles-Torres, *Appl. Catal., A* **2021**, *609*, 117905.
[15] T. Komanoya, K. Nakajima, M. Kitano, M. Hara, *J. Phys. Chem. C* **2015**, *119*, 26540.
[16] R. López-Asensio, C. P. J. Gómez, C. G. Sancho, R. Moreno-Tost, J. A. Cecilia, P. Maireles-Torres, *Int. J. Mol. Sci.* **2019**, *20*, 828.
[17] V. Montes, J. F. Miñambres, A. N. Khalilov, M. Boutonnet, J. M. Marinas, F. J. Urbano, A. M. Maharramov, A. Marinas, *Catal. Today* **2018**, *306*, 89.
[18] M. A. Aramendía, V. Borau, C. Jiménez, J. M. Marinas, J. R. Ruiz, F. J. Urbano, *Appl. Catal., A* **2003**, *244*, 207.
[19] R. Maderuelo-Solera, R. López-Asensio, J. A. Cecilia, C. P. Jiménez-Gómez, C. García-Sancho, R. Moreno-Tost, P. Maireles-Torres, *Appl. Clay Sci.* **2019**, *183*, 105351.
[20] F. Li, S. Jiang, J. Huang, Y. Wang, S. Lu, C. Li, *New J. Chem.* **2019**, *44*, 478.
[21] A. Ramanathan, M. C. C. Villalobos, C. Kwakernaak, S. Telalovic, U. Hanefeld, *Chem. - Eur. J.* **2008**, *14*, 961.
[22] F. Gonell, M. Boronat, A. Corma, *Catal. Sci. Technol.* **2017**, *7*, 2865.
[23] M. M. Antunes, S. Lima, P. Neves, A. L. Magalhães, E. Fazio, A. Fernandes, F. Neri, C. M. Silva, S. M. Rocha, M. F. Ribeiro, M. Pillinger, A. Urakawa, A. A. Valente, *J. Catal.* **2015**, *329*, 522.
[24] N. O. Popovych, P. I. Kyriienko, Y. Millot, L. Valentin, J. Gurgul, R. P. Socha, J. Żukrowski, S. O. Soloviev, S. Dzwigaj, *Microporous Mesoporous Mater.* **2018**, *268*, 178.
[25] M. Koehle, R. F. Lobo, *Catal. Sci. Technol.* **2016**, *6*, 3018.
[26] M. Boronat, A. Corma, M. Renz, *J. Phys. Chem. B* **2006**, *110*, 21168.
[27] M. J. Gilkey, B. Xu, *ACS Catal.* **2016**, *6*, 1420.
[28] T. Zhang, Y. Lu, W. Li, M. Su, T. Yang, A. Ogunbiyi, Y. Jin, *Int. J. Hydrogen Energy* **2019**, *44*, 14527.
[29] J. A. Melero, G. Morales, J. Iglesias, M. Paniagua, C. López-Aguado, *Ind. Eng. Chem. Res.* **2018**, *57*, 11592.
[30] S. Zhu, Y. Xue, J. Guo, Y. Cen, J. Wang, W. Fan, *ACS Catal.* **2016**, *6*, 2035.
[31] H. Zhang, W. Yang, I. I. Roslan, S. Jaenicke, G. K. Chuah, *J. Catal.* **2019**, *375*, 56.
[32] S. Song, L. Di, G. Wu, W. Dai, N. Guan, L. Li, *Appl. Catal., B* **2017**, *205*, 393.
[33] A. Galarneau, A. Barodawalla, T. J. Pinnavaia, *Nature* **1995**, *374*, 529.
[34] J. A. Cecilia, C. García-Sancho, E. Vilarrasa-García, J. Jiménez-Jiménez, E. Rodriguez-Castellón, *Chem. Rec.* **2018**, *18*, 1085.
[35] J. A. Cecilia, C. García-Sancho, F. Franco, *Microporous Mesoporous Mater.* **2013**, *176*, 95.

© 2022 The Authors. Advanced Sustainable Systems published by Wiley-VCH GmbH

[36] J. A. Cecilia, D. M. Soriano, A. Natoli, E. Rodríguez-Castellón, J. M. López Nieto, *Materials* **2018**, *11*, 1562.
[37] S. D. Goals (SDGs), https://sustainabledevelopment.un.org/?menu=1300 (accessed: February 2022).
[38] L. Pardo, M. Domínguez-Maqueda, J. A. Cecilia, M. P. Rodríguez, J. Osajima, M. Á. Moriñigo, F. Franco, *Minerals* **2020**, *10*, 130.
[39] P. S. Nayak, B. K. Singh, *Bull. Mater. Sci.* **2007**, *30*, 235.
[40] C. Belver, J. Bedia, J. J. Rodriguez, *Appl. Catal., B* **2015**, *176–177*, 278.
[41] J. Madejová, *Vib. Spectrosc.* **2003**, *31*, 1.
[42] V. M. Malhotra, A. A. Ogloza, *Phys. Chem. Miner.* **1989**, *16*, 386.
[43] F. Franco, J. A. Cecilia, M. Pozo, L. Pardo, E. Bellido, C. García-Sancho, *Microporous Mesoporous Mater.* **2020**, *292*, 109749.
[44] M. Thommes, K. Kaneko, A. V. Neimark, J. P. Olivier, F. Rodriguez-Reinoso, J. Rouquerol, K. S. W. Sing, *Pure Appl. Chem.* **2015**, *87*, 1051.
[45] M. L. Occelli, *Catal. Today* **1988**, *2*, 339.
[46] S. Brunauer, P. H. Emmett, E. Teller, *J. Am. Chem. Soc.* **1938**, *60*, 309.
[47] J. H. de Boer, B. C. Lippens, B. G. Linsen, J. C. P. Broekhoff, A. van den Heuvel, T. J. Osinga, *J. Colloid Interface Sci.* **1966**, *21*, 405.
[48] J. Landers, G. Y. Gor, A. V. Neimark, *Colloids Surf., A* **2013**, *437*, 3.
[49] R. S. Mikhail, S. Brunauer, E. E. Bodor, *J. Colloid Interface Sci.* **1968**, *26*, 45.
[50] J. F. Moulder, W. F. Stickle, P. E. Sobol, K. D. Bomben, *Handbook of X-Ray Photoelectron Spectroscopy, Perkin-Elmer Corporation*, Physical Electronics Division, Eden Prairie, MInnesota, USA **1992**.
[51] H. Matsuhashi, H. Motoi, K. Arata, *Catal. Lett.* **1994**, *26*, 325.
[52] A. Corma, C. Rodellas, V. Fornes, *J. Catal.* **1984**, *88*, 374.
[53] H. Miyata, J. B. Moffat, *J. Catal.* **1980**, *62*, 357.
[54] M. Trombetta, G. Busca, M. Lenarda, L. Storaro, R. Ganzerla, L. Piovesan, A. J. Lopez, M. Alcantara-Rodrìguez, E. Rodríguez-Castellón, *Appl. Catal., A* **2000**, *193*, 55.
[55] H. P. Winoto, B. S. Ahn, J. Jae, *J. Ind. Eng. Chem.* **2016**, *40*, 62.
[56] L. Bui, H. Luo, W. R. Gunther, Y. Román-Leshkov, *Angew. Chem., Int. Ed.* **2013**, *52*, 8022.
[57] J. Iglesias, J. A. Melero, G. Morales, M. Paniagua, B. Hernández, A. Osatiashtiani, A. F. Lee, K. Wilson, *Catal. Sci. Technol.* **2018**, *8*, 4485.
[58] K. D. Kim, J. Kim, W. Y. Teoh, J. C. Kim, J. Huang, R. Ryoo, *RSC Adv.* **2020**, *10*, 35318.
[59] H. P. Winoto, Z. A. Fikri, J. M. Ha, Y. K. Park, H. Lee, D. J. Suh, J. Jae, *Appl. Catal., B* **2019**, *241*, 588.
[60] J. Zhu, G. Yin, *ACS Catal.* **2021**, *11*, 10058.
[61] C. P. Jiménez-Gómez, J. A. Cecilia, R. Moreno-Tost, P. Maireles-Torres, *ChemSusChem* **2017**, *10*, 1448.
[62] M. S. Gyngazova, L. Grazia, A. Lolli, G. Innocenti, T. Tabanelli, M. Mella, S. Albonetti, F. Cavani, *J. Catal.* **2019**, *372*, 61.

© 2022 The Authors. Advanced Sustainable Systems published by Wiley-VCH GmbH